Computation theory of partially coherent imaging by stacked pupil shift matrix

Kenji Yamazoe[1,2]

[1]*Canon Inc., 23-10, Kiyohara-Kogyo-danchi, Utsunomiya-shi, Tochigi-ken, 321-3298, Japan*
[2]*Current address: 231 Cory Hall, Department of Electrical Engineering and Computer Science, University of California, Berkeley, California, 94720-1770, USA*
(kenjiy@eecs.berkeley.edu)

Received July 29, 2008; accepted September 28, 2008;
posted October 6, 2008 (Doc. ID 99478); published November 26, 2008

A theory of partially coherent imaging is presented. In this theory, a singular matrix $\mathcal{P}$ is introduced in a spatial frequency domain. The matrix $\mathcal{P}$ can be obtained by stacking pupil functions that are shifted according to the illumination condition. Applying singular-value decomposition to the matrix $\mathcal{P}$ generates eigenvalues and eigenfunctions. Using eigenvalues and eigenfunctions, the aerial image can be computed without the transmission cross coefficient (TCC). A notable feature of the matrix $\mathcal{P}$ is that the relationship between the matrix $\mathcal{P}$ and the TCC matrix $\mathbf{T}$ is $\mathbf{T}=\mathcal{P}^{\dagger}\mathcal{P}$, where † represents the Hermitian conjugate. This suggests that the matrix $\mathcal{P}$ can be regarded as a fundamental operator in partially coherent imaging. © 2008 Optical Society of America

OCIS codes: 110.4980, 110.2990, 110.5220.

1. INTRODUCTION

Partially coherent imaging was formulated by Hopkins [1] with the introduction of a four-dimensional transmission factor, or so called transmission cross coefficient (TCC) [1,2]. Hopkins's equation involves quadruple integral over the pupil plane due to the TCC. Kintner developed a numerical calculation algorithm of Hopkins's equation [3]; however, it requires large computer memory because of the four-dimensional TCC and is time-consuming due to the quadruple integral of Hopkins's equation. For the purpose of faster computation of partially coherent imaging, two types of derivative algorithms of Hopkins's equation have been introduced. One is based on physical interpretation of Hopkins's equation, and the other is based on matrix treatment of partially coherent imaging.

The physical interpretation of Hopkins's equation resulted in a point source decomposition, or so-called Abbe's method [4–6]. Partially coherent illumination can be regarded as a set of mutually incoherent point sources. Each point source forms a light intensity distribution on the image plane. The incoherent summation of all light intensity emitted by point sources creates the aerial image. Abbe's method is compatible with the well-known fast Fourier transform (FFT) algorithm and does not need the TCC, so it requires less computer memory. On the other hand, the computation speed of Abbe's method is limited by the repetition of the FFT. If there are N instances of mutually incoherent point sources, Abbe's method requires N instances of FFT. This is the most time-consuming part of Abbe's method.

Matrix treatment of partially coherent imaging has been widely studied, and the basic concept can be found in the literature [7,8]. Broadly, the matrix treatment can be divided into two categories. One is the matrix treatment of the mutual intensity in which the mutual intensity is decomposed by the Karhunen–Loeve transform [9] to remove the correlation. Wolf has further refined the decomposition method of the mutual intensity [10], and later, more complicated matrix treatments were studied [11,12]. The mutual intensity decomposition technique has been applied to partially coherent imaging, particularly in the field of optical microlithography simulation [13–15]. The mutual intensity decomposition involves integration over the object plane. Typically, the computation of the integral over the object plane requires large sampling numbers with small grid size. Therefore, although it is physically meaningful, it is not suitable for a fast computation.

The other matrix treatment that is suitable for fast computation is a decomposition of the TCC. The TCC is defined on the pupil plane. The integral over the pupil plane requires fewer sampling numbers than that over the object plane. The TCC decomposition is sometimes referred to as sum of coherent system decomposition (SOCS) [16,17]. In the SOCS, the numerical TCC array is decomposed into eigenvalues and eigenfunctions of the aerial image by singular-value decomposition (SVD). An important feature of the SOCS is that it can produce an approximate aerial image with high accuracy with the FFT having to be done fewer than N times because of the energy compaction property of the SVD. Although the SOCS settled the time-consuming aspect of Abbe's method, the SOCS does need the TCC and the SVD of the TCC. The calculation of the TCC requires large computer memory and is time-consuming because of the double integrals over the overlapping area of the effective light source, pupil function, and complex conjugate of pupil function. Furthermore, the SVD of a large matrix is also

time-consuming. Consequently, the SOCS needs large computation time and computer memory in order to generate the eigenvalues and eigenfunctions.

Since the advantage of Abbe's method is that it does not need the TCC, while the advantage of the SOCS is the reduced FFT time, one has had to choose Abbe's method or the SOCS appropriately according to the simulation purpose. Once the calculation of TCC and the SVD of the TCC are completed, the SOCS can compute the aerial image faster than Abbe's method. The TCC depends on the optical conditions, such as numerical aperture, wavelength, aberration, polarization, etc. Therefore, if one repeats the simulation for different objects without changing optical conditions, the SOCS is preferred. On the other hand, if one repeats the simulation for changing optical conditions, Abbe's method is used.

In this paper, I introduce an algorithm that does not need the TCC and can reduce the repetition of FFT. This method can be regarded as possessing the advantages of both Abbe's method and SOCS. This result is achieved by changing the analytical representation of Abbe's method to the matrix representation. In this approach, first a singular matrix $\mathcal{P}$ is derived from a pupil function and effective light source. By applying SVD to the matrix $\mathcal{P}$, eigenvalues and eigenfunctions are obtained. The aerial image can then be computed by eigenvalues and eigenfunctions. Thus one does not need the TCC matrix. Furthermore, this method requires fewer than N instances of FFT to compute the aerial image with high accuracy by virtue of the energy compaction property of the SVD.

The introduction of the matrix $\mathcal{P}$ and aerial image calculation method with the matrix $\mathcal{P}$ are explained in Section 2, where it is recognized that the calculation of the matrix $\mathcal{P}$ is quite simple. The matrix $\mathcal{P}$ can be obtained by discrete pupil function. By simply shifting the pupil function and stacking the two-dimensional pupil functions into one dimension, one can obtain each row of the matrix $\mathcal{P}$. Thus one needs neither summation nor product. I will show aerial image simulation results in Section 3, where I show the numerical calculation results with reduced FFT repetition as well. In Section 4, I discuss features of the matrix $\mathcal{P}$ and show that the relationship between $\mathcal{P}$ and the TCC matrix $\mathbf{T}$ is $\mathbf{T}=\mathcal{P}^{\dagger}\mathcal{P}$, where † represents the Hermitian conjugate. Therefore, the matrix $\mathcal{P}$ can be regarded as a fundamental matrix in partially coherent imaging.

2. THEORY

In this section, I assume a simplified optical system that consists of a light source, a condenser lens, an object, projection optics, and an image. The coordinate system on the image plane is denoted by (x,y) while the coordinate system on the light source and the pupil plane is represented by (f,g). In the computation, the number of sampling grids of the pupil is the same as that of the effective light source.

A. Numerical Form of Abbe's Method

The analytical representation of Abbe's method can be written as [4–6]

$$I(x,y)=\int\int S(f',g')|\mathbf{FT}[\hat{a}(f-f',g-g')P(f,g)]|^2\mathrm{d}f'\mathrm{d}g', \tag{1}$$

where I is the aerial image, $\hat{a}$ is an object spectrum or diffracted light amplitude, P is a pupil function, S is an effective light source, and **FT** operates the two-dimensional Fourier transform. Hereafter, since we concentrate on the discrete aerial image computation, it is helpful to rewrite the aerial image I in the discrete form

$$I(x,y)=\sum_{i,j} S(f_i',g_j')|\mathbf{FT}[\hat{a}(f-f_i',g-g_j')P(f,g)]|^2. \tag{2}$$

The meaning of Eq. (2) is as follows. A plane wave emitted from a point source (f_i',g_j') illuminates the object, and its diffracted light is shifted depending on the incidence angle of the plane wave. Then the diffracted light is cut by the pupil to form the light intensity distribution on the image plane. The incoherent sum of the light intensity emitted by each of the point sources creates the aerial image.

B. One-dimensional Matrix Representation

In this subsection, I present a matrix style of Eq. (2) with the conditions of a one-dimensional pupil and a one-dimensional effective light source. Furthermore, I assume the ideal condition of aberration-free and unpolarized illumination. Since the Fourier transform is the sum of weighted plane waves, the aerial image can be regarded as the sum of plane waves. Plane-wave $\exp(-i2\pi fx)$ is the orthogonal function with respect to different f. Therefore, it is convenient to write the set of plane waves as the bracket representation

$$|\phi^{1D}\rangle=[\exp(-i2\pi f_1x)\quad \exp(-i2\pi f_2x)\quad \cdots\quad \exp(-i2\pi f_Mx)]^T, \tag{3}$$

where T represents the transpose of the matrix and M is the number of the basis depending on the sampling points. For a simple discussion, let M be 7. The diffracted light can be represented by using Eq. (3) as

$$|\hat{a}'^{1D}\rangle=[\hat{a}_1\exp(-i2\pi f_1x)\quad \hat{a}_2\exp(-i2\pi f_2x)\quad \cdots\quad \hat{a}_7\exp(-i2\pi f_7x)]^T, \tag{4}$$

where $\hat{a}_i=\hat{a}(f_i)$ for simple notation. Suppose the pupil radius is normalized to be unity. In a usual case, one has to consider the maximum spatial frequency of 2 so that

$$(f_1\ \ f_2\ \ f_3\ \ f_4\ \ f_5\ \ f_6\ \ f_7)=\left(-2\ \ -\frac{4}{3}\ \ -\frac{2}{3}\ \ 0\ \ \frac{2}{3}\ \ \frac{4}{3}\ \ 2\right). \tag{5}$$

Note that $f_4(=0)$ is the center of the pupil. The pupil function that passes the light of $|f|\leq 1$ through the pupil can be represented by the rect(f), where rect(f)=1 if $|f|\leq 1$, otherwise zero. A matrix style of the pupil function can be written as

$$\mathbf{P^{1D}} = (0 \quad 0 \quad 1 \quad 1 \quad 1 \quad 0 \quad 0). \tag{6}$$

If a point source lies on f_4, which is the center of the effective light source, the diffracted light just after the pupil $|D^{1D}\rangle$ can be written as

$$|D^{1D}\rangle = \mathcal{P}_1^{1D}|\hat{a}'^{1D}\rangle, \tag{7}$$

where $\mathcal{P}_1^{1D}=\mathbf{P}^{1D}$. The light intensity on the image plane formed by the plane wave emitted from the point source at f_4 is the product of $|D^{1D}\rangle$ and the conjugate of $|D^{1D}\rangle$, that is $\langle D^{1D}|$; thus

$$I_1(x) = \langle D^{1D}|D^{1D}\rangle = \langle \hat{a}'^{1D}|(\mathcal{P}_1^{1D})^{\dagger}\mathcal{P}_1^{1D}|\hat{a}'^{1D}\rangle. \tag{8}$$

Next, consider the oblique incident plane wave emitted from the point source at f_5. By the oblique incident illumination, the diffracted light is shifted as expressed by Eq. (2). Here, by changing Eq. (2), we obtain

$$I(x,y) = \sum_{i,j} S(f_i',g_j')|\mathbf{FT}[\hat{a}(f,g)P(f+f_i',g+g_j')]|^2. \tag{9}$$

Equation (9) can be interpreted as the oblique incident illumination shifting the pupil without shifting the diffracted light. Therefore, a plane wave emitted from the point source at f_5 forms the light intensity on the image plane,

$$I_2(x) = \langle \hat{a}'^{1D}|(\mathcal{P}_2^{1D})^{\dagger}\mathcal{P}_2^{1D}|\hat{a}'^{1D}\rangle, \tag{10}$$

where

$$\mathcal{P}_2^{1D} = (0 \quad 1 \quad 1 \quad 1 \quad 0 \quad 0 \quad 0). \tag{11}$$

Note that $\mathcal{P}_2^{1D}$ can be obtained by simply shifting the pupil function. If the effective light source has two mutually incoherent point sources at f_4 and f_5, the aerial image I is the sum of I_1 and I_2; thus

$$\begin{aligned} I(x) &= I_1(x) + I_2(x) \\ &= \langle \hat{a}'^{1D}|(\mathcal{P}_1^{1D})^{\dagger}\mathcal{P}_1^{1D}|\hat{a}'^{1D}\rangle + \langle \hat{a}'^{1D}|(\mathcal{P}_2^{1D})^{\dagger}\mathcal{P}_2^{1D}|\hat{a}'^{1D}\rangle. \end{aligned} \tag{12}$$

From linear algebra, Eq. (12) can be rewritten as

$$I(x) = \langle \hat{a}'^{1D}|(\mathcal{P}^{1D})^{\dagger}\mathcal{P}^{1D}|\hat{a}'^{1D}\rangle, \tag{13}$$

where

$$\mathcal{P}^{1D} = \begin{pmatrix} \mathcal{P}_1^{1D} \\ \mathcal{P}_2^{1D} \end{pmatrix} = \begin{pmatrix} 0 & 0 & 1 & 1 & 1 & 0 & 0 \\ 0 & 1 & 1 & 1 & 0 & 0 & 0 \end{pmatrix}. \tag{14}$$

Equation (13) is the matrix representation of the aerial image under the one-dimensional condition. From Eq. (13), $\mathcal{P}^{1D}$ can be regarded as the operator that features the partially coherent imaging. Hereafter, $\mathcal{P}^{1D}$ is referred to as a P-operator for one-dimensional imaging. Note that each row of the P-operator for one-dimensional imaging can be obtained only by shifting the pupil function in Eq. (6); therefore, the fast P-operator calculation is possible. Furthermore, each component of the P-operator for one-dimensional imaging under an ideal condition is either one or zero.

C. Two-Dimensional Matrix Representation

In this subsection, the P-operator is extended for two-dimensional imaging under ideal imaging conditions (aberration-free and unpolarized illumination). First, let a two-dimensional plane wave be $\exp[-i2\pi(fx+gy)]$. The set of two-dimensional plane waves is

$$\phi(f,g) = \begin{pmatrix} \exp[-i2\pi(f_1x+g_1y)] & \exp[-i2\pi(f_1x+g_2y)] & \cdots & \exp[-i2\pi(f_1x+g_My)] \\ \exp[-i2\pi(f_2x+g_1y)] & \exp[-i2\pi(f_2x+g_2y)] & \cdots & \exp[-i2\pi(f_1x+g_My)] \\ \vdots & & & \\ \exp[-i2\pi(f_Mx+g_1y)] & \exp[-i2\pi(f_Mx+g_2y)] & \cdots & \exp[-i2\pi(f_Mx+g_My)] \end{pmatrix}. \tag{15}$$

For a simple discussion, let $M=7$. The two-dimensional diffracted light distribution is

$$\hat{a}'(f,g) = \begin{pmatrix} \hat{a}_{1,1}\exp[-i2\pi(f_1x+g_1y)] & \hat{a}_{1,2}\exp[-i2\pi(f_2x+g_1y)] & \cdots & \hat{a}_{1,7}\exp[-i2\pi(f_1x+g_7y)] \\ \hat{a}_{2,1}\exp[-i2\pi(f_2x+g_1y)] & \hat{a}_{2,2}\exp[-i2\pi(f_2x+g_2y)] & \cdots & \hat{a}_{2,7}\exp[-i2\pi(f_2x+g_7y)] \\ \vdots & & & \\ \hat{a}_{7,1}\exp[-i2\pi(f_7x+g_1y)] & \hat{a}_{7,2}\exp[-i2\pi(f_7x+g_2y)] & \cdots & \hat{a}_{7,7}\exp[-i2\pi(f_7x+g_7y)] \end{pmatrix}, \tag{16}$$

where $\hat{a}_{i,j}=\hat{a}(f_i,g_j)$ for simple notation. Suppose the pupil radius is unity. As in Eq. (6), the two-dimensional pupil function—which is $\mathrm{circ}(f,g)$, where $\mathrm{circ}(f,g)=1$ if $(f^2+g^2)\leq 1$, otherwise zero—is written as

$$P(f,g)=\begin{bmatrix}0&0&0&0&0&0&0\\0&0&0&0&0&0&0\\0&0&1&1&1&0&0\\0&0&1&1&1&0&0\\0&0&1&1&1&0&0\\0&0&0&0&0&0&0\\0&0&0&0&0&0&0\end{bmatrix}. \tag{17}$$

Here, I introduce a stacking operator $\mathbf{Y}$ that reshapes a two-dimensional matrix to a column vector in a certain order. For an example of the stacking operator $\mathbf{Y}$, refer to Appendix A. By the stacking operator $\mathbf{Y}$, the bracket representation of two-dimensional diffracted light is

$$|\hat{a}'\rangle=\mathbf{Y}[\hat{a}'(f,g)], \tag{18}$$

If the point source lies on $(f,g)=(0,0)$, which is the center of the effective light source, the diffracted light just after the pupil $|D\rangle$ can be written as

$$|D\rangle=\mathcal{P}_1|\hat{a}'\rangle, \tag{19}$$

where $\mathcal{P}_1=\mathbf{Y}[P(f,g)]^T$. Therefore, the light intensity on the image plane formed by plane waves emitted from the point source at $(f,g)=(0,0)$ is

$$\begin{aligned}I_1(x,y)&=\langle D|D\rangle\\&=\langle\hat{a}'|\mathcal{P}_1^\dagger\mathcal{P}_1|\hat{a}'\rangle.\end{aligned} \tag{20}$$

If there is another point source, for example at (f_2',g_2'), we can define $\mathcal{P}_2$ by stacking $P(f-f_2',g-g_2')$ as $\mathbf{Y}[P(f-f_2',g-g_2')]$ and calculate the light intensity on the image plane I_2 in a manner similar to Eq. (20). The sum of I_1 and I_2 forms the aerial image I; thus,

$$\begin{aligned}I(x,y)&=I_1(x,y)+I_2(x,y)\\&=\langle\hat{a}'|\mathcal{P}_1^\dagger\mathcal{P}_1|\hat{a}'\rangle+\langle\hat{a}'|\mathcal{P}_2^\dagger\mathcal{P}_2|\hat{a}'\rangle\\&=\langle\hat{a}'|\mathcal{P}^\dagger\mathcal{P}|\hat{a}'\rangle,\end{aligned} \tag{21}$$

where

$$\mathcal{P}=\begin{pmatrix}\mathcal{P}_1\\\mathcal{P}_2\end{pmatrix}. \tag{22}$$

If there are N kinds of point sources and the position of the ith point source is (f_i',g_i'), the P-operator for two-dimensional imaging is defined as

$$\begin{aligned}\mathcal{P}&=\begin{pmatrix}\mathbf{Y}[P(f-f_1',g-g_1')]^T\\\mathbf{Y}[P(f-f_2,g'-g_2')]^T\\\vdots\\\mathbf{Y}[P(f-f_N',g-g_N')]^T\end{pmatrix}\\&=\begin{pmatrix}\mathcal{P}_1\\\mathcal{P}_2\\\vdots\\\mathcal{P}_N\end{pmatrix},\end{aligned} \tag{23}$$

and the aerial image can be written as

$$I(x,y)=\langle\hat{a}'|\mathcal{P}^\dagger\mathcal{P}|\hat{a}'\rangle. \tag{24}$$

Equation (24) is the matrix representation of Abbe's method for two-dimensional imaging and Eq. (23) is the P-operator for two-dimensional imaging. Note that each row of the P-operator for two-dimensional imaging can be obtained by shifting the pupil function in Eq. (17), followed by stacking by stacking operator $\mathbf{Y}$, and last, transposing, leading to the fast computation. In the following, I concentrate on the two-dimensional calculation so that I refer to the P-operator for two-dimensional imaging simply as P-operator. Note that each component of the P-operator under an ideal condition is either 1 or 0.

D. Modeling of the Optical Condition

In this subsection, I extend the method to handle the aberration, apodization, and light intensity distribution and polarization state of the effective light source. First, let the aberration function and apodization function be $W(f,g)$ and $o(f,g)$, respectively. The pupil function can then be written as

$$P'(f,g)=\mathrm{circ}(f,g)o(f,g)\exp[-i2\pi W(f,g)]. \tag{25}$$

Next, suppose that the light intensity of the ith point source at (f_i',g_i') is S_i. Then, the P-operator can be written as,

$$\mathcal{P}'=\begin{pmatrix}\sqrt{S_1}\mathbf{Y}[P'(f-f_1',g-g_1')]^T\\\sqrt{S_2}\mathbf{Y}[P'(f-f_2',g-g_2')]^T\\\vdots\\\sqrt{S_N}\mathbf{Y}[P'(f-f_N',g-g_N')]^T\end{pmatrix}, \tag{26}$$

where N is the number of point sources. Using Eq. (26), we can treat the aberration, apodization, and light intensity distribution of the effective light source.

Furthermore, the polarization state can be included in the P-operator. Under the polarized illumination condition, one can define three kinds of pupil function P^x, P^y, and P^z [18–20]. Each pupil function defines P-operators $\mathcal{P}^x$, $\mathcal{P}^y$ and $\mathcal{P}^z$:

$$\mathcal{P}^l=\begin{pmatrix}\sqrt{S_1}\mathbf{Y}[P^l(f-f_1',g-g_1')P'(f-f_1',g-g_1')]^T\\\sqrt{S_2}\mathbf{Y}[P^l(f-f_2',g-g_2')P'(f-f_2',g-g_2')]^T\\\vdots\\\sqrt{S_N}\mathbf{Y}[P^l(f-f_N',g-g_N')P'(f-f_N',g-g_N')]^T\end{pmatrix}, \tag{27}$$

where l is x, y, and z. The full P-operator with aberration, apodization, and light intensity distribution and polarization state of the effective light source can be written as

$$\mathcal{P}_{full}=\begin{pmatrix}\mathcal{P}^x\\\mathcal{P}^y\\\mathcal{P}^z\end{pmatrix}. \tag{28}$$

If the number of point sources is N, the number of rows for the full P-operator is $3N$.

E. Numerical Calculation Algorithm

In this subsection, the aerial image calculation algorithm with P-operator is presented. The aerial image can be obtained with P-operator in Eq. (24), and I write it again:

$$I(x,y) = \langle \hat{a}' | \mathcal{P}^{\dagger} \mathcal{P} | \hat{a}' \rangle. \tag{29}$$

Note that $\mathcal{P}$ is not a square matrix but an $N \times M^2$ singular matrix. Applying the SVD to $\mathcal{P}$, one obtains

$$\mathcal{P} = \mathbf{U} \mathbf{\Lambda} \mathbf{V}^{\dagger}. \tag{30}$$

where $\mathbf{U}$ is a unitary matrix and $\mathbf{\Lambda}$ is a diagonal matrix with real and positive diagonal elements [21]. $\mathbf{U}$ and $\mathbf{\Lambda}$ are $N \times N$ matrices and $\mathbf{V}$ is an $M^2 \times N$ matrix. As a property of $\mathbf{V}$, $\mathbf{V}^{\dagger}\mathbf{V}$ is an $N \times N$ identity matrix. Substituting Eq. (30) into Eq. (29), one obtains

$$\begin{aligned} I(x,y) &= \langle \hat{a}' | \mathbf{V} \mathbf{\Lambda} \mathbf{U}^{\dagger} \mathbf{U} \mathbf{\Lambda} \mathbf{V}^{\dagger} | \hat{a}' \rangle \\ &= \langle \hat{a}' | \mathbf{V} \mathbf{\Lambda}^2 \mathbf{V}^{\dagger} | \hat{a}' \rangle. \end{aligned} \tag{31}$$

Therefore, one can calculate the aerial image using eigenvalues and eigenfunctions of the P-operator. Each row of $\mathbf{V}^{\dagger}$ represents the stacked eigenfunction. Let the ith row of $\mathbf{V}^{\dagger}$ be $\mathbf{V}_i^{\dagger}$. By inverse-stacking $\mathbf{V}_i^{\dagger}$, one can obtain N kinds of eigenfunction $\mathbf{\Phi}_i$; that is $\mathbf{\Phi}_i = \mathbf{Y}^{-1}[(\mathbf{V}_i^{\dagger})^T]$. The final equation for the numerical calculation is

$$I(x,y) = \sum_{i=1}^{N} \lambda_i^2 |\mathbf{FT}[\hat{a}(f,g)\mathbf{\Phi}_i(f,g)]|^2, \tag{32}$$

where λ_i is the ith row and ith column element of $\mathbf{\Lambda}$. The number of eigenvalues or eigenfunctions is N (or $3N$ if the polarization is considered) as explained in Section 4. Using Eq. (32), we can compute the aerial image without the TCC.

3. EXAMPLE OF NUMERICAL SIMULATIONS

In this section, I show numerical calculation results under the ideal conditions (aberration-free and unpolarized illumination) and review the calculation method with illustrations. In this simulation, the range of f and g is from -2 to 2 and the number of sampling points M is set to 63. Hence, $f_1 = g_1 = -2$, $f_{63} = g_{63} = 2$, and $\Delta f = \Delta g = 4/63$. The numerical aperture of the projection optics is 0.86 and the exposure wavelength is 248 nm.

First, the object and the illumination shape are illustrated in Fig. 1. The amplitude $\hat{a}$ of the light diffracted by the normally incident plane wave is illustrated in Fig. 2. The calculated P-operator is illustrated in Fig. 3.

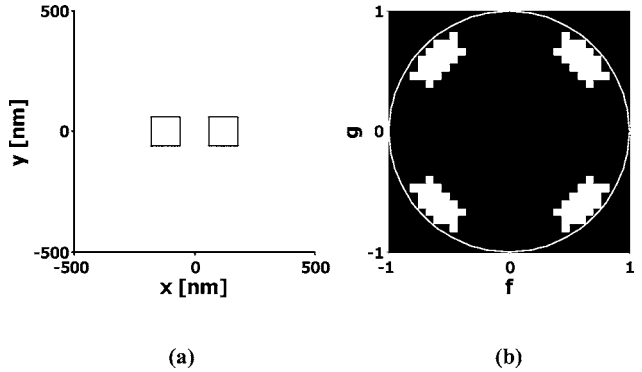

Fig. 1. Target object and the illumination shape. (a) The target object is two clear apertures 100 nm square in an opaque background. (b) Schematic view of illumination shape; each pixel shows the mutually incoherent point source.

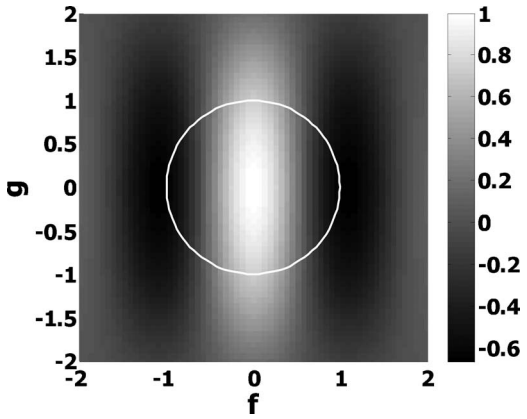

Fig. 2. Diffracted light amplitude computed from the object illustrated in Fig. 1(a) under normal incident illumination. The maximum value is normalized to unity. The white circle indicates the pupil.

The illumination illustrated in Fig. 1 contains 92 mutually incoherent point sources. Hence, the number of the rows of the P-operator is 92. Since the number of sampling points is 63, the number of the columns of the P-operator is $63^2 = 3969$. By applying the SVD to the P-operator, we can obtain 92 kinds of eigenvalues and eigenfunctions as explained below in Section 4.

After sorting the eigenvalues in descending order, the eigenvalues are plotted in Fig. 4. Eigenvalues decrease rapidly as the eigenvalue number increases. In [22], Bastiaans proposed that uncertainty for partially coherent light takes its minimum when the modal expanded eigenvalue of the partially coherent illumination is $2\sigma/(1+\sigma) \times [(1-\sigma)/(1+\sigma)]^i$, where $0 < \sigma < 1$. Figure 4 evidences the tendency of his proposal. However, note that since λ_2 equals λ_3, the second and third states are the degeneracy states.

As examples, only $\mathbf{\Phi}_1$, $\mathbf{\Phi}_2$, and $\mathbf{\Phi}_3$ are plotted in Fig. 5. Since the second and third eigenfunctions are degeneracy states, they are symmetrical. The Fourier transforms of $\hat{a}\mathbf{\Phi}_1$, $\hat{a}\mathbf{\Phi}_2$, and $\hat{a}\mathbf{\Phi}_3$ are plotted in Fig. 6, which are the eigenfunctions of the aerial image. The summation of

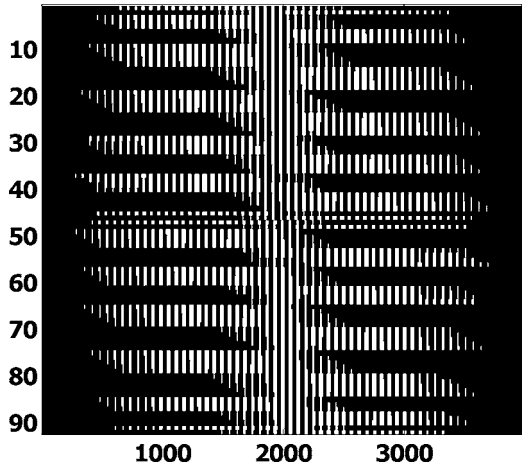

Fig. 3. The P-operator computed under the ideal conditions. The ith row and jth column of the discrete pupil function is stacked on the $[(i-1) \times M + j]$th element by the stacking operator $\mathbf{Y}$. A white cell is 1 and a black cell is 0.

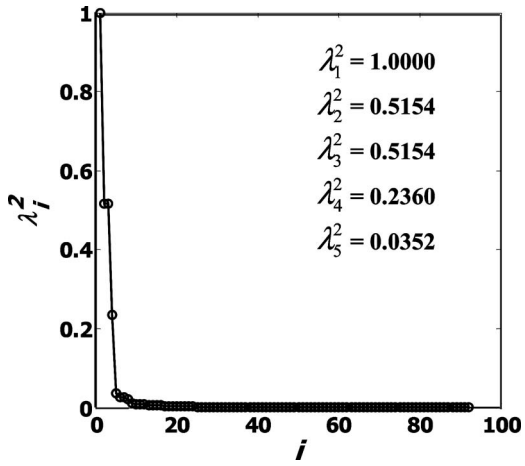

Fig. 4. Eigenvalue computed from the P-operator shown in Fig. 3. After sorting the eigenvalues in descending order, the eigenvalues are normalized for λ_1 to be unity. The explicit eigenvalues up to λ_5 are listed.

$\lambda_i^2|\mathbf{FT}[\hat{a}\mathbf{\Phi}_i]|^2$ forms the final aerial image, as illustrated in Fig. 7. In this calculation, the sampling number of the fast Fourier transform (FFT) is set to 1024. The result is compared to that of the numerical representation of Abbe's method [Eq. (2)] and was verified to have good correspondence.

In the following, I show the high-accuracy aerial image approximation with reduced FFT repetition. As mentioned above, we need 92 instances of FFT to obtain the complete aerial image. Here, from Fig. 4, note that the eigenvalue decreases rapidly as the eigenvalue number increases. This means higher orders of eigenfunctions have little impact on the aerial image formation and can be ignored. For example, if we use only nine kinds of eigenfunction, we can obtain the approximate aerial image shown in Fig. 8. The difference between the complete aerial image shown in Fig. 7 and the approximate aerial image shown in Fig. 8 is plotted in Fig. 9. The difference is at most 2.0×10^{-3}. Note that the most time-consuming part of the functional representation of Abbe's method is the repetition of the FFT. By this method, the FFT repetition can be reduced significantly with high accuracy approximation.

Next, let us compare the computation time with SOCS. The SOCS requires the TCC matrix. The TCC matrix calculation itself is time-consuming as explained later in Subsection 4.A. Furthermore, since the size of the TCC matrix is $M^2\times M^2$ (in this example, 3969×3969), the TCC matrix is a large matrix and therefore it takes a long time to do a SVD of the TCC matrix. On the other hand, this computation needs the P-operator, which can be computed faster than the TCC matrix. Furthermore, the size of the P-operator is $N\times M^2$ (in this example, 92×3969),

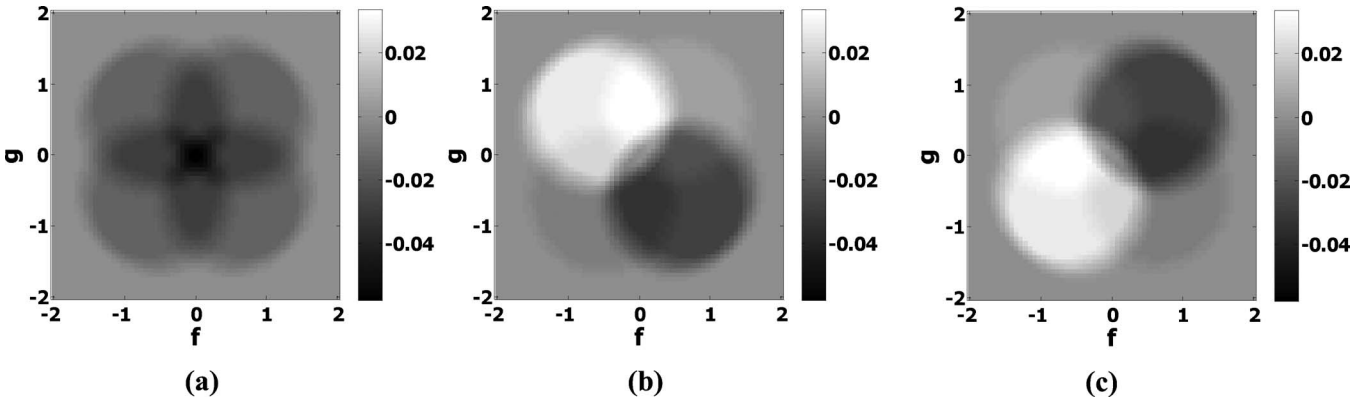

Fig. 5. Eigenfunctions computed from the P-operator shown in Fig. 3. (a) First eigenfunction $\mathbf{\Phi}_1$, (b) second eigenfunction $\mathbf{\Phi}_2$, (c) third eigenfunction $\mathbf{\Phi}_3$.

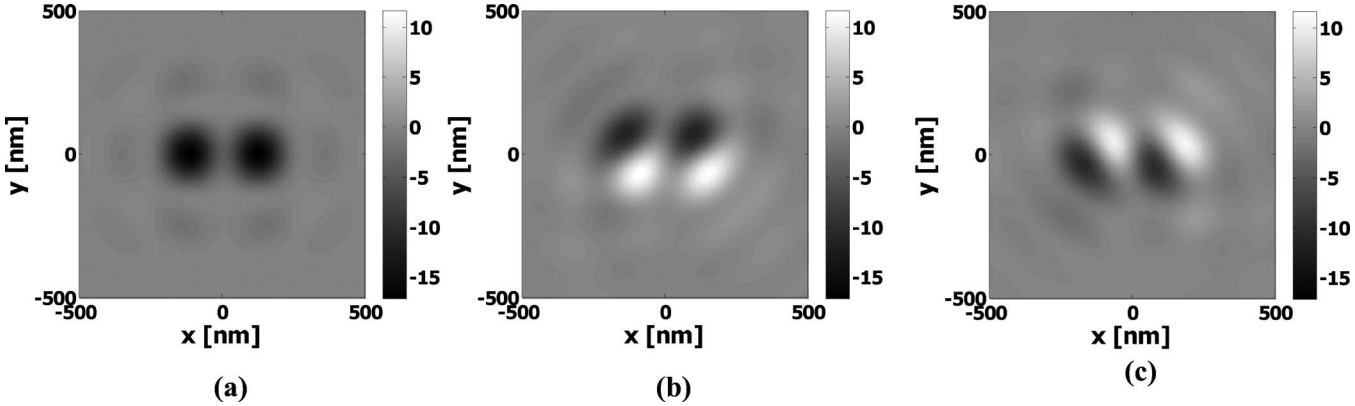

Fig. 6. Eigenfunctions of the aerial image. (a) First eigenfunction $\mathbf{FT}[\hat{a}\mathbf{\Phi}_1]$. (b) The second eigenfunction is a pure imaginary number so that the imaginary part of $\mathbf{FT}[\hat{a}\mathbf{\Phi}_2]$ is plotted. (c) The third eigenfunction is the pure imaginary number so that the imaginary part of $\mathbf{FT}[\hat{a}\mathbf{\Phi}_3]$ is plotted.

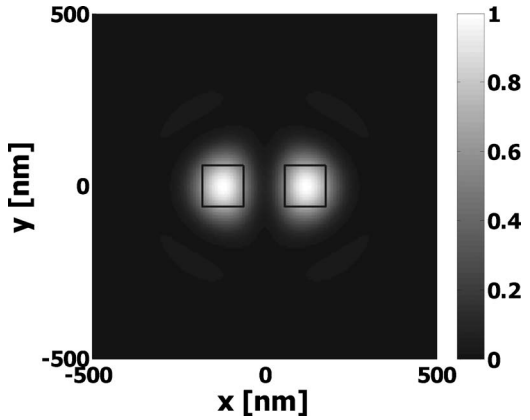

Fig. 7. Final aerial image computed by Eq. (32). The maximum value is normalized to unity.

which is always less than the TCC matrix. Therefore, a faster SVD of the P-operator is possible. For example, the computation time of the TCC matrix was 429 s while that of the P-operator was less than 0.1 s. The SVD of the TCC matrix took 385 s while that of the P-operator took 0.3 s. Hence, this method realizes a faster computation of the aerial image than SOCS.

The total aerial image computation time of the SOCS with nine kinds of eigenfunction is 827 s. Abbe's method takes 92 instances of FFT, resulting in 20 s to compute the aerial image. In this method, it takes 3 s to obtain the approximate aerial image with nine kinds of eigenfunction.

The above computations were performed on a 2.99 GHz Opteron with MATLAB. The operating system was Windows XP/64.

4. DISCUSSION

A. Relationship between TCC and P-Operator

The relationship between the TCC matrix and the matrix $\mathcal{P}$ is derived in this subsection. Hopkins's equation describers the partially coherent imaging as [1,2],

$$I(x,y) = \iint \mathrm{TCC}(f',g',f'',g'')\hat{a}(f',g')\hat{a}^*(f'',g'') \times \exp\{-i2\pi[(f'-f'')x + (g'-g'')y]\}\mathrm{d}f'\mathrm{d}g'\mathrm{d}f''\mathrm{d}g'', \tag{33}$$

where the TCC is represented as

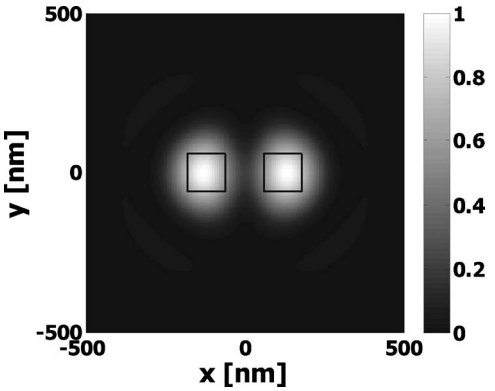

Fig. 8. Approximate aerial image with nine kinds of eigenvalues and eigenfunctions. The maximum value is normalized to unity.

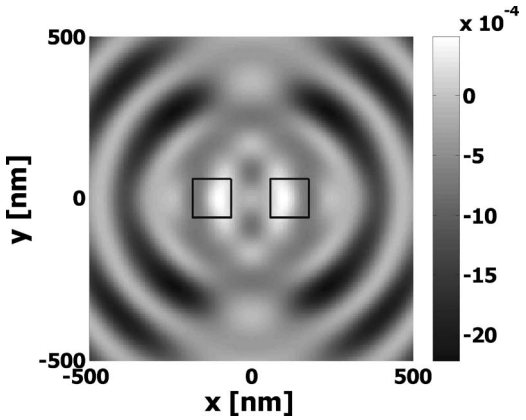

Fig. 9. Difference of Fig. 8 and Fig. 7; approximate aerial image minus complete aerial image.

$$\mathrm{TCC}(f',g',f'',g'') = \iint S(f,g)P(f+f',g+g') \times P^*(f+f'',g+g'')\mathrm{d}f\mathrm{d}g. \tag{34}$$

For a simple discussion, the one-dimensional computation of Eq. (33) is

$$\begin{aligned} I(x) &= \sum_{i,j} [\hat{a}^*(f_j)\exp(i2\pi f_j x)]\mathrm{TCC}^{1D}(f_i,f_j)[\hat{a}(f_i) \times \exp(-i2\pi f_i x)] \\ &= \sum_{i,j} [\hat{a}(f_j)\exp(-i2\pi f_j x)]^*\mathrm{TCC}^{1D}(f_i,f_j) \times [\hat{a}(f_i)\exp(-i2\pi f_i x)]. \end{aligned} \tag{35}$$

The matrix representation of Eq. (35) can be obtained as

$$\begin{aligned} I(x) &= \sum_j \hat{a}'^*(f_j)\left[\sum_i \mathrm{TCC}^{1D}(f_j,f_i)\hat{a}'(f_i)\right] \\ &= \langle \hat{a}'|\mathbf{T}^{1D}|\hat{a}'\rangle, \end{aligned} \tag{36}$$

where $\mathbf{T}^{1D}$ is the TCC array for one-dimensional imaging. Comparison of Eq. (36) with Eq. (13) leads to

$$\mathbf{T}^{1D} = (\mathcal{P}^{1D})^\dagger \mathcal{P}^{1D}. \tag{37}$$

Equation (37) can be extended to two-dimensional imaging, and we obtain

$$\mathbf{T} = \mathcal{P}^\dagger \mathcal{P}. \tag{38}$$

That is, TCC *matrix* $\mathbf{T}$ *is the product of* $\mathcal{P}^\dagger$ *and* $\mathcal{P}$. This result leads to the fast TCC matrix computation. The conventional calculation of the TCC matrix is done with Eq. (34). The calculation of Eq. (34) is time-consuming because of the double integral. However, TCC computation time is significantly reduced with Eq. (38), because Eq. (38), is the simple product of the two matrices, and the computation of the P-operator is a simple shift of the pupil function without any summation or product procedure.

The reduction of the TCC computation is a critical issue in an optical microlithography simulation, and some methods are introduced in [23]. The calculation by Eq. (38) is, to my knowledge, the fastest numerical TCC calculation method. For example, given the effective light source shown in Fig. 1(b), the calculation of the TCC ma-

trix by Eq. (34) took 429 s. On the other hand, it took less than 0.1 s to calculate the P-operator and 0.9 s to calculate the TCC matrix by Eq. (38). The above computations were performed by the same platform as that of Section 3.

B. Number of Eigenvalues or Eigenfunctions

The number of the eigenvalues or eigenfunctions of TCC matrix required to form the complete aerial image is derived in this subsection. The maximum number of eigenvalues of the TCC matrix is shown in [24,25]; however, the explicit number of eigenvalues is not shown there. The explicit number of eigenvalues of the TCC matrix is derived as follows. First, the number of the eigenvalues of the TCC matrix is rank($\mathbf{T}$). Let $\mathbf{F}$ and $\mathbf{G}$ be arbitrary matrices. The rank($\mathbf{FG}$) is min[rank($\mathbf{F}$),rank($\mathbf{G}$)] from linear algebra. Therefore, without accounting for polarization, we obtain

$$\begin{aligned}\mathrm{rank}(\mathbf{T}) &= \min[\mathrm{rank}(\mathcal{P}^{\dagger}),\mathrm{rank}(\mathcal{P})]\\ &= \min[N,N]\\ &= N.\end{aligned} \tag{39}$$

Thus, in an unpolarized condition, the number of the eigenvalues of the TCC matrix corresponds to the number of the point sources of the effective light source. If we consider the polarized illumination, the number of the eigenvalues of the TCC matrix is $3N$. The increased number of eigenvalues can be interpreted in terms of the degree of freedom being increased by three times when the polarization is included.

5. CONCLUSION

The matrix representation of partially coherent imaging has been presented. In this method, a singular matrix $\mathcal{P}$ is introduced. Each row of the matrix $\mathcal{P}$ is derived by shifting the discrete pupil function according to the oblique incident light of the illumination, followed by stacking the two-dimensional pupil matrix into one dimension. Each component of the matrix $\mathcal{P}$ is either 1 or 0 under an ideal imaging condition. By applying SVD to the matrix $\mathcal{P}$, we can obtain eigenvalues and eigenfunctions. Using eigenvalues and eigenfunctions, the aerial image can be computed without the TCC. In this method, optical effects, such as aberration, pupil apodization, polarization, and light intensity distribution of the source, can be modeled. The relationship between the TCC matrix $\mathbf{T}$ and the matrix $\mathcal{P}$ is derived and shown to be $\mathbf{T}=\mathcal{P}^{\dagger}\mathcal{P}$. Thus, the matrix $\mathcal{P}$ models for the TCC matrix $\mathbf{T}$. By using this relationship, fast TCC matrix computation was demonstrated. Furthermore, the number of eigenfunctions of the TCC matrix is shown to be the same as the number of point sources that compose the partially coherent illumination. Some numerical calculation examples were shown, and the fast computation method was also demonstrated.

APPENDIX A

In this appendix, an example of the stacking and inverse stacking operator is shown. Assume the following matrix:

$$\mathbf{A}=\begin{bmatrix} a & b & c\\ d & e & f\\ g & h & i\end{bmatrix}. \tag{A1}$$

The stacking operation $\mathbf{Y}$ of the matrix $\mathbf{A}$ and the resulting matrix $\mathbf{B}$ are related as

$$\mathbf{Y}[\mathbf{A}]=\begin{pmatrix} a\\ b\\ c\\ d\\ e\\ f\\ g\\ h\\ i\end{pmatrix}, \tag{A2}$$

$$=\mathbf{B},$$

$$\mathbf{Y}[\mathbf{A}]^{T}=(a\quad b\quad c\quad d\quad e\quad f\quad g\quad h\quad i)=\mathbf{B}^{T}. \tag{A3}$$

Supposing $\mathbf{B}$ is an $N^2\times 1$ matrix, the inverse stacking $\mathbf{Y}^{-1}$ of the $\mathbf{B}$ generates an $N\times N$ matrix $\mathbf{A}$ as

$$\mathbf{Y}^{-1}[\mathbf{B}]=\mathbf{A}. \tag{A4}$$

These are the operations of the stacking and inverse stacking operator.

ACKNOWLEDGMENTS

I express my gratitude to Yoshiyuki Sekine and Tokuyuki Honda for technical discussion. I thank Minoru Yoshii, Akiyoshi Szuki, and Shigeyuki Uzawa for their support in this study.

REFERENCES

1. H. H. Hopkins, "On the diffraction theory of optical image," Proc. R. Soc. London, Ser. A **217**, 408–432 (1953).
2. M. Born and E. Wolf, *Principles of Optics*, 6th ed. (Pergamon, 1980), Chap. 10.
3. E. Kintner, "Method for the calculation of partially coherent imagery," Appl. Opt. **17**, 2747–2753 (1978).
4. R. Barakat, "Partially coherent imagery in the presence of aberrations," Opt. Acta **17**, 337–347 (1970).
5. M. Yeung, "Modeling aerial images in two and three dimensions," in *Proc. Kodak Microelectronics Seminar: Interface '85, Kodak Publ. G-154* (Eastman Kodak, 1986), pp. 115–126.
6. A. K. Wong, *Optical Imaging in Projection Microlithography*, A. R. Weeks, Jr., ed. (SPIE, 2005), Chap 8.
7. H. Gamo, "Matrix treatment of partial coherence," in *Progress in Optics, Vol. III*, E. Wolf, ed. (North-Holland, 1964), Chap. 3.
8. E. L. O'Neill, *Introduction to Statistical Optics* (Dover, 2003), Chap. 8.
9. J. W. Goodman, *Statistical Optics*, 1st ed. (Wiley-Interscience, 1985), pp. 109–111.
10. E. Wolf, "New spectral representation of random sources and the partially coherent fields that they generate," Opt. Commun. **38**, 3–6 (1981).
11. B. E. A. Saleh and M. Rabbani, "Simulation of partially

coherent imagery in the space and frequency domains and by modal expansion," Appl. Opt. **21**, 3770–3777 (1982).
12. H. M. Ozaktas, S. Yüksel, and M. A. Kutay, "Linear algebraic theory of partial coherence: discrete fields and measures of partial coherence," J. Opt. Soc. Am. A **19**, 1563–1571 (2002).
13. R. von Bünau, G. Owen, and R. F. W. Pease, "Depth of focus enhancement in optical lithography," J. Vac. Sci. Technol. B **10**, 3047–3054 (1992).
14. Y. C. Pati and T. Kailath, "Phase-shifting masks for microlithography: automated design and mask requirements," J. Opt. Soc. Am. A **11**, 2438–2452 (1994).
15. R. J. Socha and A. R. Neureuther, "Propagation effects of partial coherence in optical lithography," J. Vac. Sci. Technol. B **14**, 3724–3729 (1996).
16. R. J. Socha, "Propagation effects of partially coherent light in optical lithography and inspection," Ph.D. dissertation (Electronics Research Laboratory, University of California, Berkeley, 1997).
17. N. B. Cobb, "Fast optical and process proximity correction algorithms for integrated circuit manufacturing," Ph.D. dissertation (Electrical Engineering and Computer Science, University of California, Berkeley, 1998).
18. M. Mansuripur, "Certain computational aspects of vector diffraction problems," J. Opt. Soc. Am. A **6**, 786–805 (1989).
19. M. Mansuripur, "Certain computational aspects of vector diffraction problems: erratum," J. Opt. Soc. Am. A **10**, 382–383 (1993).
20. K. Adam, Y. Granik, A. Torres, and N. Cobb, "Improved modeling performance with an adapted vectorial formulation of the Hopkins imaging equation," Proc. SPIE **5040**, 78–91 (2003).
21. W. H. Press, S. A. Teukolsky, W. T. Vetterling, and B. P. Flannery, *Numerical Recipes in C*, 2nd ed. (Cambridge U. Press, 1994), Chap. 2.
22. M. J. Bastiaans, "Uncertainty principle and informational entropy for partially coherent light," J. Opt. Soc. Am. A **3**, 1243–1246 (1986).
23. R. Köhle, "Fast TCC algorithm for the model building of high NA lithography simulation," Proc. SPIE **5754**, 918–929 (2005).
24. A. Starikov, "Effective number of degrees of freedom of partially coherent source," J. Opt. Soc. Am. **72**, 1538–1544 (1982).
25. C. Zuniga and E. Tejnil, "Heuristics for truncating the number of optical kernels in Hopkins image calculation for model-based OPC treatment," Proc. SPIE **6520**, 65203l-1–14 (2007).